Experimental study of falling film evaporation in tube bundles of doubly-enhanced, horizontal tubes

Pu-Hang Jin[a], Zhuo Zhang[a], Ibrahim Mostafa[a], Chuang-Yao Zhao[b], Wen-Tao Ji[a], Wen-Quan Tao[a,*]

[a] Key Laboratory of Thermo-Fluid Science and Engineering of Ministry of Education, Xi'an Jiaotong University, Xi'an 710049, PR China
[b] School of Building Services Science and Engineering, Xi'an University of Architecture and Technology, Xi'an 710055, PR China

HIGHLIGHTS

- FFE heat transfer in tube bundle of doubly-enhanced boiling tube is characterized.
- Bundle effect is considerable for bottom tubes when heat flux exceeds 20 kW/m^2.
- Upward vapor flow deteriorates the heat transfer and worsens dryout.

ARTICLE INFO

ABSTRACT

Falling film evaporation (FFE) involves complicated physical phenomena and mechanisms such as wavy liquid film, bubbly flow, capillary-driven evaporation and nucleate boiling. FFE heat transfer characteristics in four doubly-enhanced tube bundles were investigated experimentally with R134a. For single tube, heat transfer coefficient (HTC) first increases then decreases with increase in heat flux, the turning points occurs around 20 kW/m^2. Tubes with different positions in tube bundle own similar HTCs when tested individually. In tube bundle, with decreasing film Reynolds number (Re_Γ), HTC firstly keeps a quasi-plateau stage (increasing or keeping constant for upper tubes, decreasing for lower tubes), then after a certain threshold film Reynolds number, HTC decreases sharply with Re_Γ. At lower heat fluxes (10 kW/m^2 and 20 kW/m^2), tubes with different positions exhibit similar HTCs and threshold Re_Γ. At higher heat fluxes (30 kW/m^2 and 40 kW/m^2), bottom tubes own much smaller HTCs and larger threshold Re_Γ than upper ones due to partial dryout occurrence. The tube bundle with top plate exhibits higher HTCs and lower threshold Re_Γ than those of the open-ended tube bundle indicating that counter-current vapor flow can deteriorate the heat transfer of FFE. Effect of heat flux on the bundle-averaged HTC increases with tube pitch.

1. Introduction

Environmental issues and sustainable development around the world have called for more energy saving and environment friendly refrigeration and air-conditioning devices. Falling film evaporator is known as an essential component in petrochemical industry, food processing, desalination and OTEC (ocean thermal energy conversion) systems. In the last two decades, it has been gradually implemented in water chiller, heat pump or ORC (Organic Rankine Cycle) systems as a potential substitute to pool boiling evaporator due to its several intrinsic advantages [1]. It enables the heat transfer with smaller temperature difference, the refrigeration system with less refrigerant charge, smaller size and easier oil removal. Despite the aforementioned merits, its design experience is still limited compared with its flooded

type counterpart since the effects of some fundamental parameters on falling film evaporation (FFE) heat transfer characteristics have not been revealed clearly, especially for those using enhanced tubes and at tube bundle level.

The basic working process of horizontal type FFE is that falling liquid film (refrigerant or some other working medium) evaporates at tubes' outer surfaces and cools the chilled water flowing inside the tubes. Numerous technical papers have been recently published about this subject. For single plain and enhanced tube, the influences of surface structure, surface roughness, surface material, heat flux, saturation temperature, refrigerant property and oil mixture on FFE heat transfer have been studied thoroughly [2–8]. R134a provides around 2–3 times of heat transfer coefficients of R123 for both plain and enhanced tubes [2]. Effect of heat flux on FFE heat transfer heavily depends on the

---

* Correspondent author.
E-mail address: wqtao@mail.xjtu.edu.cn (W.-Q. Tao).

Nomenclature

A	Area, m^2
D	Diameter of tube, mm
FFE	Falling film evaporation
FH	Fin height on tube outer surface, μm
h	Heat transfer coefficient/HTC, $W/m^2 \cdot K$
L	Tested length of tube, mm
PB	Pool boiling
Q	Heat transfer rate, W
q	Heat flux, kW/m^2
R	Thermal resistance, $m^2 \cdot K/W$
r	Latent heat, J/kg
Re_Γ	Film Reynolds number
T	Temperature, °C
U	Overall heat transfer coefficient, $W/m^2 \cdot K$
V	Velocity of water, m/s

Greek

Δ	Variable differential
Γ	Liquid film flow rate on one side of the tube per unit length, kg/m·s
μ	Dynamic viscosity, kg/m·s
δ	Tube wall thickness, mm
λ	Thermal conductivity, W/m·K

Subscript

ave	Average
c	Condensation
e	Evaporation
f	Fouling
Gni	Gnielinski equation
l	Liquid refrigerant
v	Vapor refrigerant
LM	Logarithmic mean value
i	Inside of tube
m	Tube number
o	Outside of tube
p	Pump
r	Reference
sat	Saturation
tot	Total
w	Wall
in	Water inlet
out	Water outlet

refrigerant type and enhanced structure [2,3]. Effect of saturation temperature on heat transfer is negligible for both single tube and tube bundle with boiling enhanced surface [3]. Empirical correlations for heat transfer prediction of single plain tube have been proposed in [4,5]. The enhanced tube performed better in falling film evaporation than pool boiling at heat flux less than 30 kW/m^2, while it began to perform poorer than pool boiling at higher heat flux [6]. Increases in surface roughness were found to increase falling film boiling heat transfer coefficients; dryout threshold was shown to increase as heat flux was increased and surface roughness and material had no discernible influence on dryout threshold [7]. FFE heat transfer can be enhanced by increasing oil concentration for both smooth and fin tubes because the bubble nucleation is enhanced by the foam [8]. Visualization study shows that bubbles can be observed in the liquid film at higher heat flux condition [5,8].

Following is a brief literature review on the falling film evaporation of refrigerant in horizontal tube bundle, focusing on the most recent publications. Ribatski and Jacobi [1] and Fernández-Seara and Pardiñas [9] gave two critical and detailed reviews on FFE heat transfer and pointed out that bundle depth effects related to liquid maldistribution and partial dryout remain unclear and avoiding dryout and deterioration of the HTCs need to be studied further. Appearance of local dryout do not necessarily causes the declining in HTC [1]. Local HTCs at the midpoint of each tube in a vertical tube array were measured by Roques and Thome [10]. In their study, a transition film Reynolds number (above which HTC is nearly insensitive to Re_Γ while HTC drops sharply below a specific value) was identified to separate the effect of Re_Γ on HTCs. They indicated that the effect of heat flux on HTCs was positive for plain tubes and negative for enhanced tubes. Their results showed that heat transfer performance of three tube arrays (with different tube pitches) was close to each other. Further, Habert and Thome [11] conducted their test in a three-row triangular pitch tube bundle (30 tubes). For the single column tube array, results are in agreement with those of Roques and Thome [10]. Bundle effect was quite evident and detrimental to heat transfer because of the nonuniformity of liquid film distribution in the tube bundle. Very scattered data among tubes in the tube bundle are shown and the effect of film Reynolds number and heat flux on HTC varies for different tubes. However, in the study of Christians and Thome [12], tube bundle effect showed little influence

on the averaged FFE heat transfer performance. HTCs of 10 tubes were not shown separately in this study and few data under lower heat fluxes (less than 20 kW/m^2) were available in their studies due to high measurement uncertainty of the thermocouples.

Tube-local HTCs were also measured by Chien and Tsai [13] and Chien and Chen [14] using R245fa and R134a respectively. Three types of tube (smooth, fin and mesh tube) in a vertical array comprised of 3 tubes were tested. HTCs increase with increase in heat flux in general; fluid temperature and film flow rate have minor influences on HTC before dry-out occurs. For the enhanced boiling tube (mesh tube), HTCs of the bottom tube are significantly lower than upper ones due to poor wetting of the bottom one.

Ji et al. [15] studied the effect of countercurrent vapor flow on falling film evaporation HTCs in a single column tube bundle with R134a. The vapor flow with a velocity of 0–3.1 m/s was created by an electrically heated boiler and the tubes tested were enhanced boiling tube with effective length of 575 mm. Falling film evaporation HTCs were found to be insensitive to heat flux for the enhanced tubes. The effect of vapor flow was complicated, varied with tube position, heat flux and film flow rate and could be neglected at lower velocity. The top two tubes were more likely to be enhanced by vapor flow. The effect of vapor shear stress may be neglected in practical engineering design at lower vapor velocity.

Comprehensive study of falling film evaporation in tube bundle was performed by Zhao et al. [16–18] using R134a. Average heat transfer coefficient of the tube bundle decreases with increase in heat flux, and higher saturation temperature benefits the heat transfer performance. At higher cross-ward vapor velocity, the vapor would have a considerable shear stress on the flowing thin liquid film and even disrupt it to induce some dry-out area. With increase in downward vapor stream velocity, HTCs first increase then decrease in general and heat transfer of upper tubes tends to be enhanced while lower tubes deteriorated.

Based on the above review, it's clear that the FFE in tube bundle is much more complicated and effects of influencing parameters are still confusing, especially the bundle effect and vapor flow. The objectives of the present study are to study how the heat flux and film flow rate affect the heat transfer performance collaboratively, to compare the HTCs of tubes with different positions in the tube bundles and to study the effects of tube pitch and vapor flow direction on the FFE HTCs in tube

bundle. FFE heat transfer data in tube bundle with industrial standard tube pitch were obtained in the present study. Considering the large tube length (about 1.5 m) and small heat flux (lower than 20 kW/m^2), the data are scarce within previous literature to the best of authors' knowledge. Further, HTCs under inverse vapor flow (generated in tube bundle) directions were compared which is barely studied before. Tube average HTC was measured with relatively low uncertainty because of large tube length (larger inlet and outlet temperature difference) and high resolution RTDs (less uncertainty in measurement of inlet and outlet temperature difference). Last, with the method suggested in this paper, tube bundle averaged HTCs were compared and analyzed.

2. Experimental system

2.1. Experimental facility

The experimental system is shown in Fig. 1. It consists of three circulation loops, heating water circuit, chilling water circuit and refrigerant circuit. The bottom vessel is served as condenser and refrigerant reservoir. Liquid refrigerant is pumped to the top of the evaporator and sprayed onto the horizontal tube's outer surface. Liquid refrigerant is heated by heating water flowing inside the tube and evaporates. Refrigerant vapor generated in the evaporator comes back to the condenser and becomes liquid again. The two water tanks can be cooled by the refrigerator or heated by the electrical heater to reach the desired temperature.

A digital pressure gauge is employed to measure the pressure in the evaporator which is taken as the saturation pressure. Mass flow rate of refrigerant is measured by Coriolis effect mass flow meter; while volume flow rate of water inside each tube is measured by electromagnetic flow meter. Platinum Resistance Thermometers are arranged at the inlet and outlet of each tube to detect temperatures. Specifications of measurement instruments are shown in Table 1. More details about the test system can be found in [3].

2.2. Test section

The liquid refrigerant flow path was separated into four branches

after the pump and mass flow meter; each branch has a ball valve to adjust the flow rate. Since the test was conducted bundle by bundle, only one valve was open when running the test system. Schematic diagram of the test section is shown in Fig. 2. Four types of tube bundles (named A1, A2, B and C) were constructed in the test section which were separated by insulation plates. The plates are made of quartz glass and equipped with dummy half tubes of the same diameter and tube pitch with the tube bundle. It should be noted that tubes shown in Fig. 2(b) are the half dummy tubes and the tested tubes are to be inserted into the space between two dummy tube columns. Industry-standard pitch was used, as shown in Table 2. They were all comprised of 6 boiling-enhanced tubes in which the top-most one was served as part of the liquid distributor. Different from other three tube bundles, column A1 (Fig. 2(c)) has two slots on top plate from which vapor generated in the tube bundle can escape. The top plates of column A2, B and C (Fig. 2(d)) were closed which forced the vapor to flow in line with the liquid film and escape from the bottom. And the differences between the three columns are in their vertical and horizontal tube pitches (see Table 2).

The same liquid distributor was adopted for each tube bundle. As shown in Fig. 2(e), it comprised of two rectangular boxes, which serve as the preliminary and secondary distributor respectively. The second one has no top plate which enable the liquid fall only under gravity. Orifices with diameter of 2.0 mm and spacing of 15.0 mm were drilled at the bottom surface of the second box which are in vertical line with the top-most points of the tested tubes. With the same diameter and pitch, two rows of orifices were drilled at the bottom plate of the top box. The liquid distributor height is about 6 mm from the bottom surface to the dummy tube above the tube bundle.

The tubes tested are doubly-enhanced boiling copper tubes, i.e., both the outside and inner side of the tube have some enhanced structure. The scanning pictures of the enhancement structure and detailed parameters are shown in Fig. 3 and Table 3. The tubes were fixed on two end plates of the evaporator by expansion. R134a was used as the working fluid and its thermo-physical properties were obtained from [19].
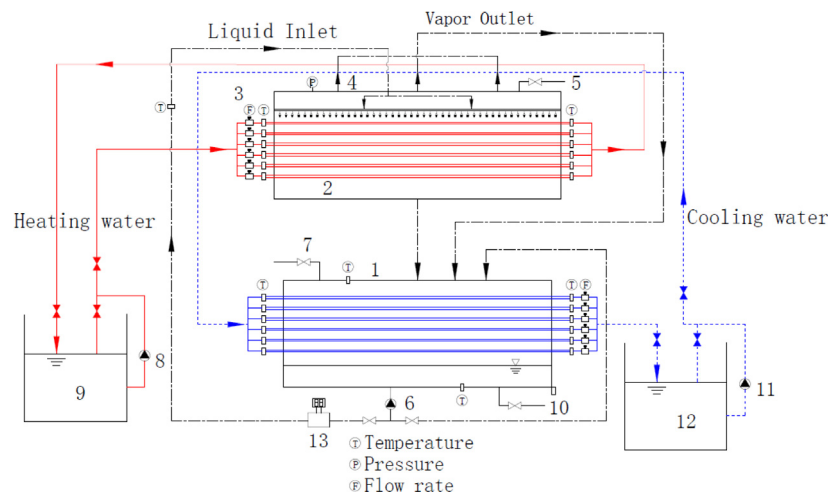
1. Condenser (reservoir); 2. Evaporator; 3. Electromagnetic flowmeter; 4. Pressure gauge; 5. Exhausting valve; 6. Refrigerant magnetic pump; 7. Refrigerant charging valve; 8. Heating water pump; 9.Hot water tank; 10. Refrigerant outlet; 11. Cooling water pump; 12. Cooling water tank; 13. Refrigerant mass flow meter.

Fig. 1. Schematic diagram of the experimental apparatus.

Table 1
Specifications of key measurement instruments.

Instruments	Specification	Precision	Range
Mass flow meter	SIEMENS MASS2100	0.1%	0–5000 kg·h^{-1}
Volume flow meter	SIEMENS MAGFLO MAG5100W	0.1%	0–3000 L·h^{-1}
Pressure gauge	KELLER LEX1	0.05%	–0.1–2.0 Mpa
RTDs	OMEGA Pt100 1/10 DIN	$\pm (0.03 + 0.0005|T|)$°C	0–60 °C
Data acquisition	Keithley digital voltmeter	0.1 μV	1000 V
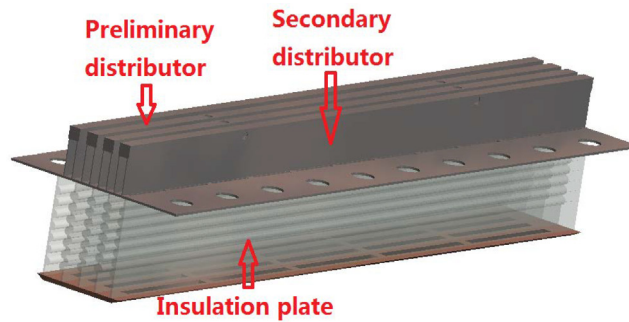
(a) Design picture of the test section
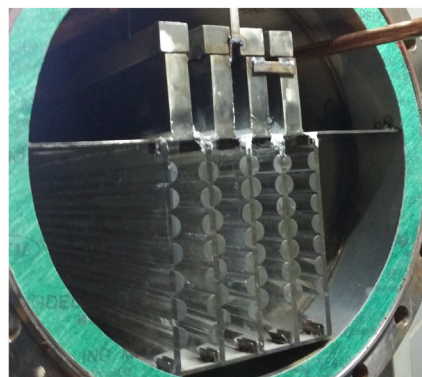
(b) Installation picture of the test section
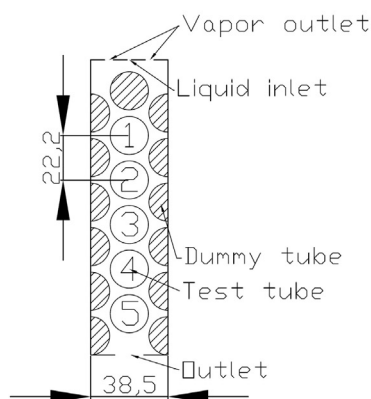
(c) Layout of the column A1   (d) Layout of column A2, B and C   (e) Diagram of the liquid distributor
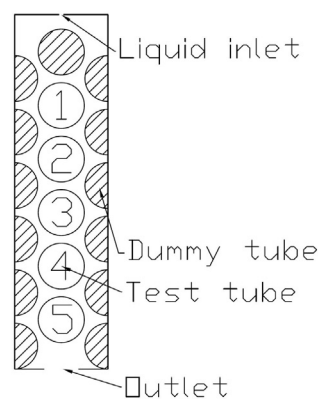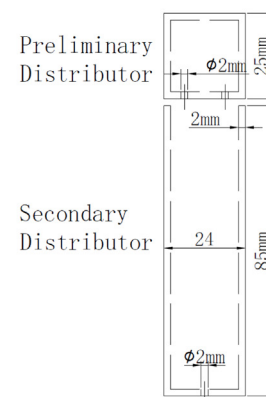
Fig. 2. Diagram of the test section.

Table 2
Parameters of four tube bundles.

Tube Bundle	A1	A2	B	C
Vertical tube pitch (mm)	22.2	22.2	23.8	25.4
Horizontal tube pitch (mm)	38.5	38.5	41.2	44

2.3. Test procedure

After the installation of the test section, high-pressure nitrogen was charged into the system until the absolute pressure reached around 1.2 MPa. Leakage test was considered satisfactory when the pressure loss was less than 1 kPa after 72 h. After that, the system was evacuated

(a) Top view of outer surface

(b) Cross section picture
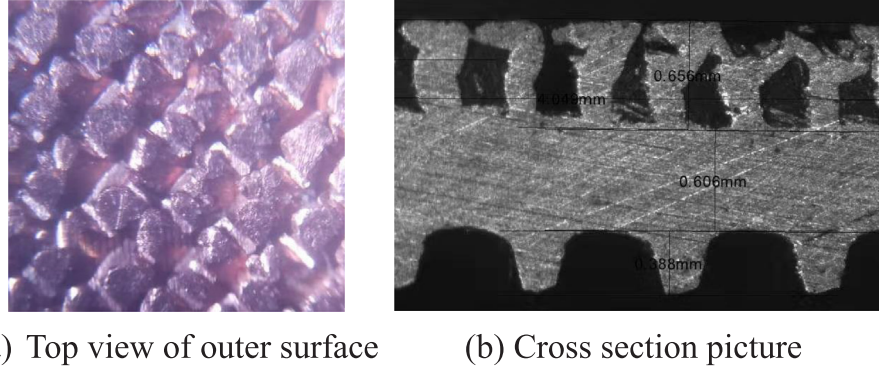
Fig. 3. Microstructure of the doubly-enhanced boiling tube.

Table 3
Geometric parameters of the test tubes.

L (mm)	δ (mm)	D_i (mm)	D_o (mm)	λ (W/m·K)	Fpi	FH (µm)
1520	1.265	16.33	18.86	339.2	50	650

by a vacuum pump until the absolute pressure is no more than 800 Pa. Then a small quantity of refrigerant was charged into the system first, then evacuated again. This step was repeated three times before the final charging of refrigerant.

The pressure in the evaporator was served as an indicator of the desired saturated temperature. Often, it took 2 h to reach the equilibrium condition which is identified by that pressure in evaporator is close to the desired saturation pressure within ± 200 Pa and the variation of heating and cooling water inlet temperature is within 0.03 K for at least 5 mins. A group of 10 data was saved for each point.

3. Date reduction method and uncertainty analysis

3.1. Heat transfer rate and heat balance

Heat transfer rate dissipated by the heating water and absorbed by the chilling water is calculated by Eqs. (1) and (2) respectively:

$$Q_{e,m} = \dot{m}_{e,m} c_p (T_{e,in,m} - T_{e,out,m}) \tag{1}$$

$$Q_{c,m} = \dot{m}_{c,m} c_p (T_{c,out,m} - T_{c,in,m}) \tag{2}$$

where the subscript "m" is the tube number, $\dot{m}_{e,m}$ and $\dot{m}_{c,m}$ are mass flow rate of heating water and chilling water respectively and c_p is the specific heat capacity of water inside the tube evaluated at the mean temperature of inlet and outlet.

For the test data here, heat balance deviation is less than 5% and shown in Eq. (3):

$$(Q_e + Q_p - Q_c)/Q_r \leqslant 5\% \tag{3}$$

where Q_e and Q_c are the overall heat transfer rate of evaporator and condenser respectively, Q_p is the power of the refrigerant pump which is immersed in the bulk of liquid refrigerant; Q_r is the reference heat transfer rate, defined by Eq. (4):

$$Q_r = (Q_e + Q_c + Q_p)/2 \tag{4}$$

For the canned motor pump, part of pumped liquid is used to cool the motor and this part of liquid is heated and vaporized; the generated vapor will return to the condenser without being carried to the liquid distributor. The pump power can be converted into three kinds of energy: internal energy, kinetic energy and potential energy of refrigerant. Careful calculation shows that less than 1% of the pump power was used to accelerate and lift the refrigerant to the top of evaporator. So that all the power of canned pump Q_p is added to the

input power of the test system in conjunction with the heating power Q_e from the hot water going through the evaporator.

3.2. Overall heat transfer coefficient of tube

The overall heat transfer coefficient evaluated at the outer surface of the tube can be calculated by Eq. (5):

$$U_m = \frac{Q_{e,m}}{A_{o,m} \Delta T_{LM,m}} \tag{5}$$

where $A_{o,m}$ is the outer surface area of the tube, $\Delta T_{LM,m}$ is the logarithm mean temperature difference between water and refrigerant saturation temperature.

$\Delta T_{LM,m}$ is defined by Eq. (6):

$$\Delta T_{LM,m} = \frac{(T_{e,in,m} - T_{e,out,m})}{\ln[(T_{e,in,m} - T_{sat})/(T_{e,out,m} - T_{sat})]} \tag{6}$$

where T_{sat} is the saturation temperature of the refrigerant which is corresponding to the vaporization pressure in the evaporator.

3.3. Evaporation heat transfer coefficient

The overall thermal resistance of a tested tube can be expressed as Eq. (7):

$$\frac{1}{U_m} = \frac{1}{h_{o,m}} + R_{w,m} + R_{f,m} + \frac{1}{c_i h_{i,m}} \frac{D_{o,m}}{D_{i,m}} \tag{7}$$

where $h_{o,m}$ is the falling film evaporation (FFE) heat transfer coefficient, $R_{w,m}$ is the thermal resistance of the tube wall, $R_{f,m}$ is the fouling thermal resistance, $h_{i,m}$ is the water side convective heat transfer coefficient calculated by Gnielinski correlation [20,21], c_i is the enhancement factor of the inner surface, and $D_{i,m}$ and $D_{o,m}$ are the inner and outer diameter of the tested tubes, respectively. Fouling thermal resistance is neglected since the tested tubes were cleaned before installation.

Hence, the FFE heat transfer coefficient can be determined by Eq. (8):

$$h_{o,m} = \left[\frac{1}{U_m} - R_{w,m} - \frac{1}{c_i h_{i,m}} \frac{D_{o,m}}{D_{i,m}} \right]^{-1} \tag{8}$$

It should be noted that the heat transfer coefficient obtained above is the average value of the tubes' outer surface.

3.4. Heat flux, film Reynolds number and average FFE HTC of tube bundle

Heat flux in the following presentation is the average heat flux evaluated on the tubes' outer surface. What should be pointed out here is that in the tube bundle test, we take the heat flux of the tube No.1 as that of the tube bundle.

$$q_{o,m} = \frac{Q_{e,m}}{A_{o,m}} \tag{9}$$

Film Reynolds number is defined by Eq. (10):

$$\mathrm{Re}_\Gamma = \frac{4\Gamma}{\mu_1} \tag{10}$$

where Γ is the film flow rate on one side of the tested tube per unit length, μ_l is the dynamic viscosity of the liquid refrigerant at the specific saturation temperature. Film Reynolds number is determined individually for each tube in the same bundle as below.

For each column, Re_Γ of tube No.1 is calculated by the film flow rate measured by the mass flow meter, while Re_Γ of tubes No. 2 to No. 5 is calculated by Eq. (11):

$$\mathrm{Re}_{\Gamma,m} = \mathrm{Re}_{\Gamma,m-1} \frac{2Q_{e,m-1}}{r \cdot L \cdot \mu_1} \tag{11}$$

where $Q_{e,m-1}$ is heat transfer rate of the upper tube, r is the latent heat, L is tube length.

The average heat transfer coefficient of tube bundles is a desired parameter to evaluate tube bundle global heat transfer performance. Here, the tube bundle average heat transfer coefficient is defined by Eq. (12):

$$h_{o,ave} = Q_{tot} / \sum_{m=1}^{5} \frac{Q_{e,m}}{h_{o,m}} \tag{12}$$

where Q_{tot} is the total heat transfer rate of the tube bundle.

3.5. Uncertainty analysis

The test for determination of the heat exchange between water and environment was done after refrigerant was charged into the system. The environmental temperature is around 15 °C during the test. Our preliminary test shows that without evaporation on the tube outside surfaces, the difference of inlet and outlet temperature of heating water was less than $\pm$ 0.03 K from 6 °C to 30 °C which shows that the heat loss to the environment can be neglected when calculating heat transfer rate from water enthalpy differences.

In most cases, the water velocity inside tube was kept at 2 m/s which is a common in a real water chiller. While when the heat flux is equal or lower than 15 kW/m², the water velocity was adjusted to around 1 m/s which aims to control the measurement uncertainty caused by low temperature difference between inlet and outlet.

Uncertainty of $h_{o,m}$ was estimated using the method suggested in [22–26]. The accuracy for determining water side heat transfer coefficient is quoted to be within 10% [27]. The estimated uncertainty of k_m is less than 6.2% for all data and the maximum uncertainty of FFE heat transfer coefficient, $h_{o,m}$, is within $\pm$ 25%. The measurement uncertainty of 72.7% data is within 15% and 78.6% within 20%. The large uncertainty occurs at low heat fluxes where the temperature difference between inlet and outlet and heat transfer temperature difference between water and refrigerant are both small. Details of the uncertainty analysis has been shown by Zhao [28]. Uncertainty of the average heat transfer coefficient of tube bundles was also analyzed based on Eq.(12), and results show that the maximum uncertainty is $\pm$ 27.3%. The measurement uncertainty range obtained is comparable with previous references adopting Wilson plot for data reduction [2,6,7,11,12].

4. Experimental results

Before the HTC measurement test, the enhancement factor of tube inner surface was obtained by Wilson plot method [24]. Then, tests were conducted column by column to study FFE heat transfer characteristics in tube bundle and the effects of several influencing parameters (heat flux, film flow rate, tube position, tube pitch and vapor flow direction) on heat transfer. Test results and analysis are shown
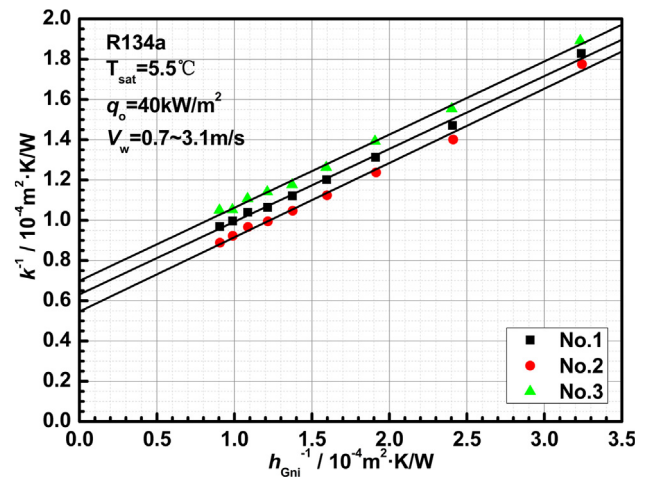

Fig. 4. Results of Wilson plot method.

below in order.

4.1. Determination of the enhancement factor of the inner surface

Enhancement factor of the internal surface was obtained by Wilson plot method [24] to calculate the water side HTC, and the results are shown in Fig. 4. Tests were conducted on three tubes separately to get the internal enhancement factor of each tube. The measured results are listed in Table 4 and the average value 3.1 is taken as the enhancement factor for each tube in four tube bundles.

4.2. Experimental results of single tube

To evaluate the differences of heat transfer performance of tubes positioned in upper or lower part of the tube bundle, tests for single tube were conducted row by row in column C at the heat flux of 40 kW/m² and three film Reynolds numbers. Only the tested tube was heated by hot water during the test, which means that the tested tube can be regarded as the first tube with heat transfer and the tubes above it only serve as the liquid distributor.

Test results are shown in Fig. 5. As a whole, the figure indicates that the HTCs of the all 5 tubes fluctuate within a region with its maximum relative width about 25%. Generally speaking, the variation of tube HTC at different position can be attributed to different falling film impact and liquid distribution uniformity. In this regard, tube positions No. 1, No. 3, and No. 5 have favorable effects and such effects are weak at position No. 4. The effect of film Reynolds number is negligible, showing that the HT process may be dominated by boiling mechanism.

Fig. 6 shows the variation trend of HTCs with heat flux, tests were conducted under two specific film Reynolds numbers. The first curve (Re_Γ = 1600, (Reverse)) was obtained with the heat flux decreased step by step. The other two curve were measured with increasing heat flux.

In general, HTC increases first then decreases gently with further increase in heat flux. This trend suggests the transition from convective dominated heat transfer to nucleate boiling dominated one. At the larger film Reynolds number of 1600, two curves exhibit very close HTCs when the heat flux is larger than 80 kW/m². The "Reverse" curve shows slight lower HTCs from 20 kW/m² to 80 kW/m², while larger ones when the heat flux is less than 20 kW/m². The cause may be that

Table 4
Enhancement factor of water side heat transfer coefficient.

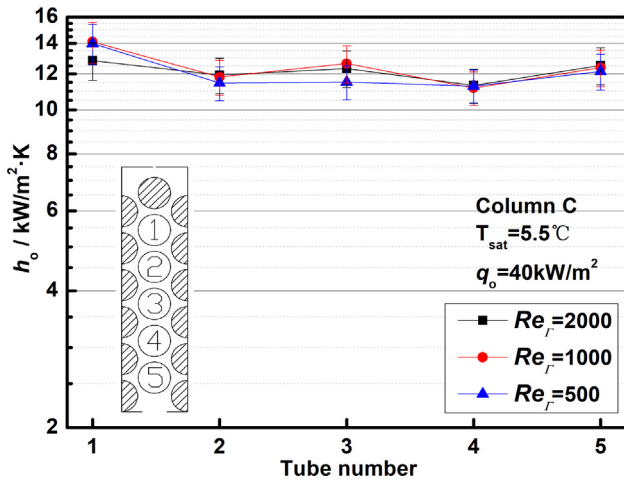| Tube number	No.1	No.2	No.3	Average
Enhancement factor c_i	3.125	3.063	3.11	3.1

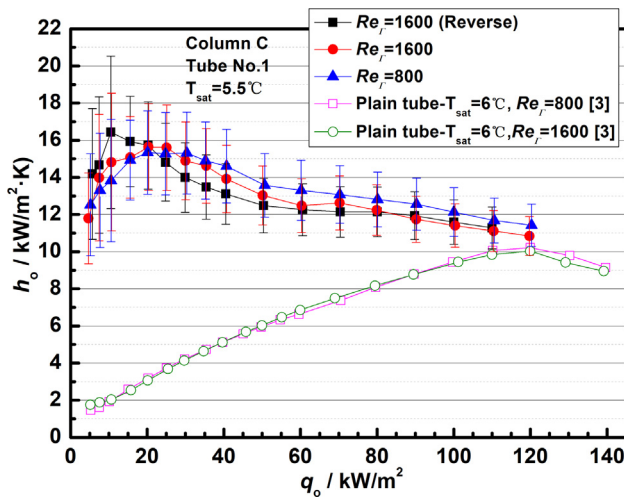Fig. 5. HTCs comparison of single tube in column C.

Fig. 6. HTCs comparison between plain tube (in Ref. [3]) and the boiling enhanced tube (Tube No.1 in column C).

the nucleation sites remained active when tests were performed with descending heat flux. The results with higher film Reynolds number ($Re_{\Gamma} = 1600$) show slightly larger HTCs than those with lower ($Re_{\Gamma} = 800$) in the low heat-flux range, but the trend is the opposite at higher heat fluxes. At lower heat fluxes, convection and evaporation dominate the heat transfer process and larger film flow rate can intensify the convection and film vibration. At larger heat fluxes, nucleate boiling is dominant, thinner liquid film at smaller film Reynolds number can facilitate the escape of induced vapor in reentrant cavities. Comparison with the plain tube shows that at lower heat flux which is the enhanced surface designed for, the structured surface has a considerable enhancement in heat transfer. When heat flux is about 120 kW/m² they have much more close HTCs, which suggests very severe dryout occurs within the enhancement structures. Considering the extended heat transfer area of the boiling enhanced tube, the proportion of dryout area should be higher than that of the plain surface.

4.3. Experimental results of tube bundle

This part shows the test results of four tube bundles. Experiments were conducted under four heat fluxes (10, 20, 30 and 40 kW/m²) at the same saturation temperature of 5.5 °C. The heat flux of tube No.1 was regarded as the nominal heat flux of the tube bundle. All the heat transfer coefficient data are plotted versus local film Reynolds number, calculated by Eqs. (10) and (11).

Figs. 7–10 show the HTC variation trend of each tube with Re_{Γ} in four tube bundles A1, A2, B and C, respectively. From these figures, several features should be noted as followings.

1) Most curves exhibit similar HTC variation trend with decrease in film Reynolds

   number, a quasi-plateau stage (wetting regime) at larger film Reynolds number and a sharp decrease stage (dryout regime) when the film Reynolds number is less than a certain value. Specifically speaking, HTCs of upper tubes first keep constant or increase gradually with decreasing Re_{Γ}, then decrease sharply. For bottom tubes, their HTCs show a consistent diminishing variation trend, especially at higher heat fluxes (30 and 40 kW/m²).

2) Generally speaking, the differences between tube HTCs of different positions for the same tube bundle increase with heat flux, especially at low film Reynolds number region. Except the lowest heat flux, the magnitudes of tube HTCs are in the same order as the tube positions, i.e., an appreciable descending trend from position 1 to position 5 can be observed. As indicated above the heat flux values are nominal for tube positions of No. 2 to 5, and only for tube No. 1 it is the actual value. With the increase in heat flux the descending trend of tube heat flux from top to bottom of the same column becomes more appreciable, leading to more significant differences between different tubes. While the descending trend of HTC with bundle depth is not as sharp as that of reference [17]; for example, HTC difference among tubes is about 14.8% while more than 60% in [17] when $q_{o} = 20$ kW/m² and $Re_{\Gamma} \approx 1400$, as shown in Fig. 8(b).

3) As far as the threshold film Reynolds number is concerned, the top tube should be taken as the representative one since both heat flux and film Reynolds number are its actual ones. Then it can be clearly seen from the figures that, for column A1 it is around $Re_{\Gamma} = 600$, for A2 around 300, for B around 300 and for C around 400 to 500.

4) For the lowest heat flux in test, i.e., $q_{o} = 10$ kW/m², for the four tube bundles tested the tube HTC of the top one is not the largest, while that of 2nd position generally ranks first. When $q_{o} \geq 20$ kW/m², the 1st tube usually performs best.

The differences of HTCs between column A1 and A2 may be attributed to the difference of the top plate. For A1 there are two vapor outlets (top and bottom), while for A2 the only vapor outlet is at the bottom. Thus, most vapor will escape from the top of the tube bundle in column A1. While for column A2, vapor can only go out through the bottom, leading to a lower lifting vapor velocity in the tube column. The ascending refrigerant vapor will decelerate the falling liquid film, leading to a reduced impinging effect, less uniform liquid distribution and more entrainment, especially on the lower tubes. Thus, the HTC differences among tubes of column A1 are larger than those of column A2, especially under testing conditions of high heat flux.

To further compare the differences of heat transfer performance among tube bundles, comparison of bundle average HTCs, obtained by Eq. (12), is shown in Figs. 11 and 12.

1) For the four tube bundles, in quasi-plateau stage bundle average HTCs increase with heat flux, showing that it is in the boiling mechanism dominated region.

2) Generally speaking, the HTCs of column A2 are higher than those of A1, which is consistent with above discussion on the differences between the tube HTCs of A1 and A2.

3) As far as the bundle threshold film Reynolds number is concerned, A1 has almost the same value (around 600) for different heat fluxes while for A2 it varies from 300 to 400 for $q_{o} = 10$ kW/m² to around 900 for $q_{o} = 40$ kW/m²;

4) From Fig. 12, we can see that column A2, B and C exhibit more or less similar HTC variation trend and the bundle threshold film

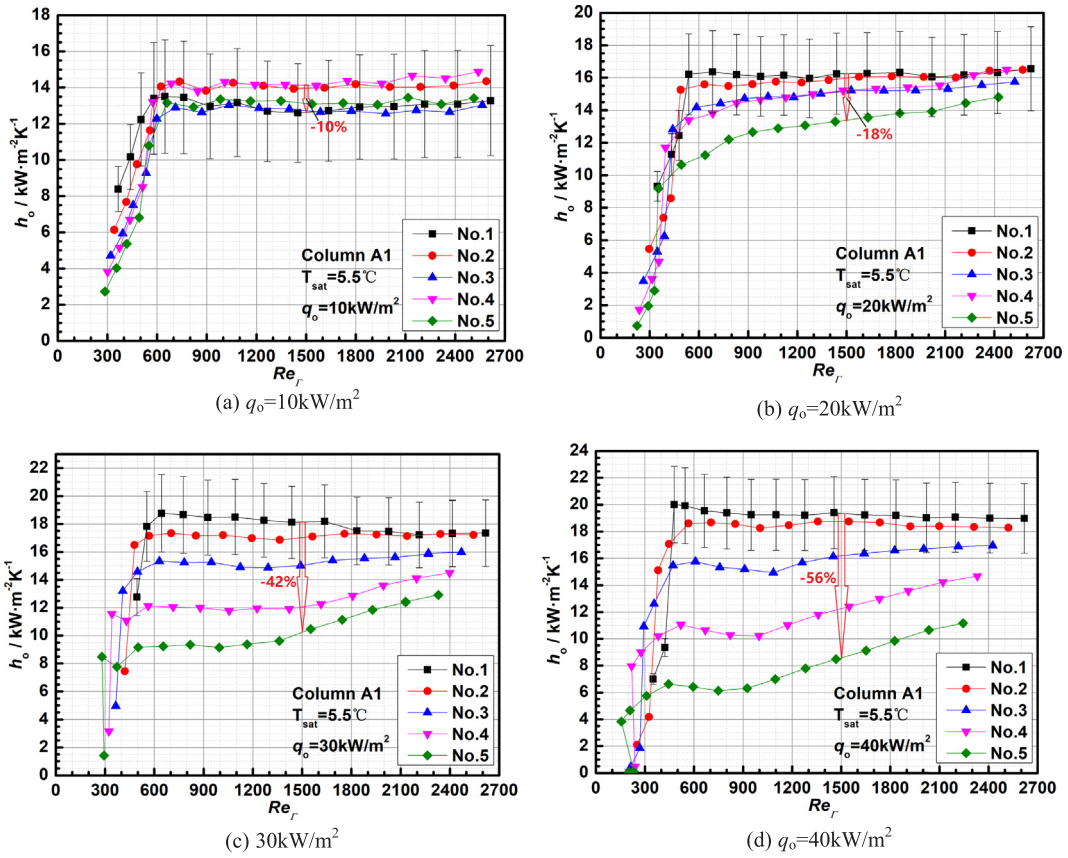(a) q_o=10kW/m^2

(b) q_o=20kW/m^2

(c) 30kW/m^2

(d) q_o=40kW/m^2

Fig. 7. Variation trend of HTCs with film Reynolds number of column A1.

(a) q_o=10kW/m^2

(b) q_o=20kW/m^2

(c) q_o=30kW/m^2

(d) q_o = 40 kW/m^2

Fig. 8. Variation trend of HTCs with film Reynolds number of column A2.

(a) q_o = 10 kW/m²   (b) q_o = 20 kW/m²
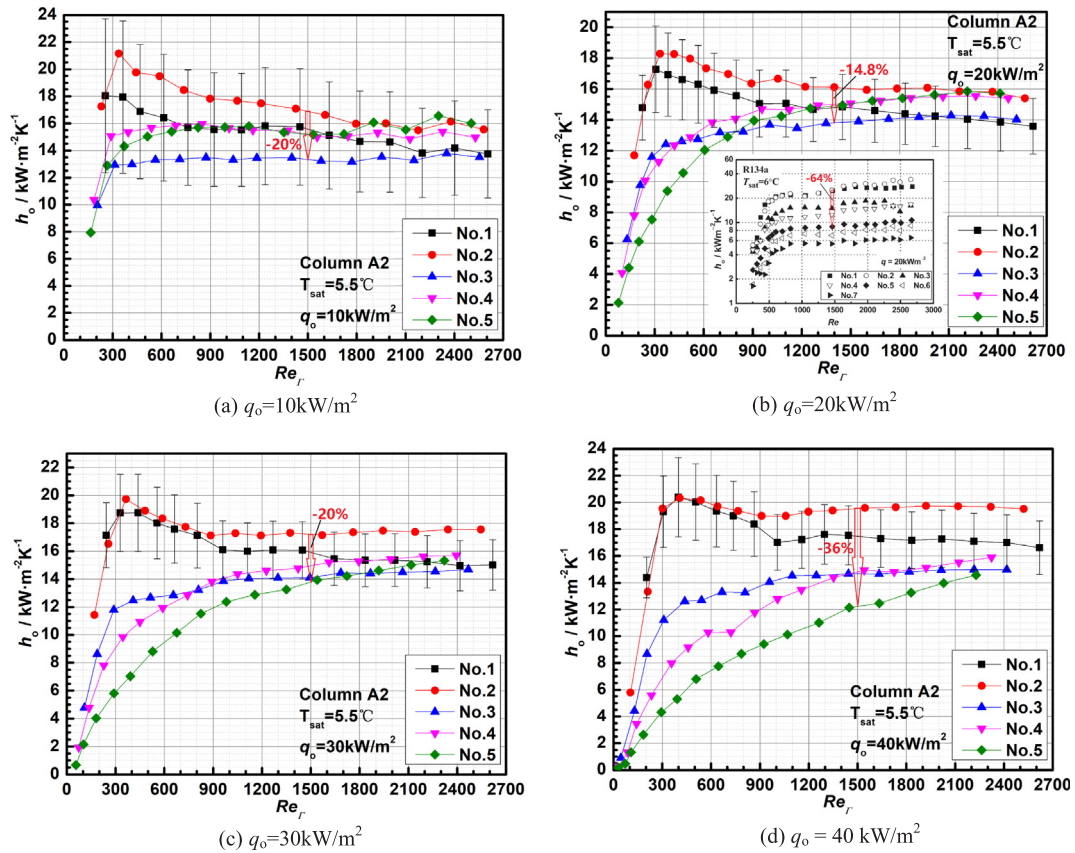
(c) q_o = 30 kW/m²   (d) q_o = 40 kW/m²

Fig. 9. Variation trend of HTCs with film Reynolds number of column B.

(a) q_o = 10 kW/m²   (b) q_o = 20 kW/m²

(c) q_o = 30 kW/m²   (d) q_o = 40 kW/m²
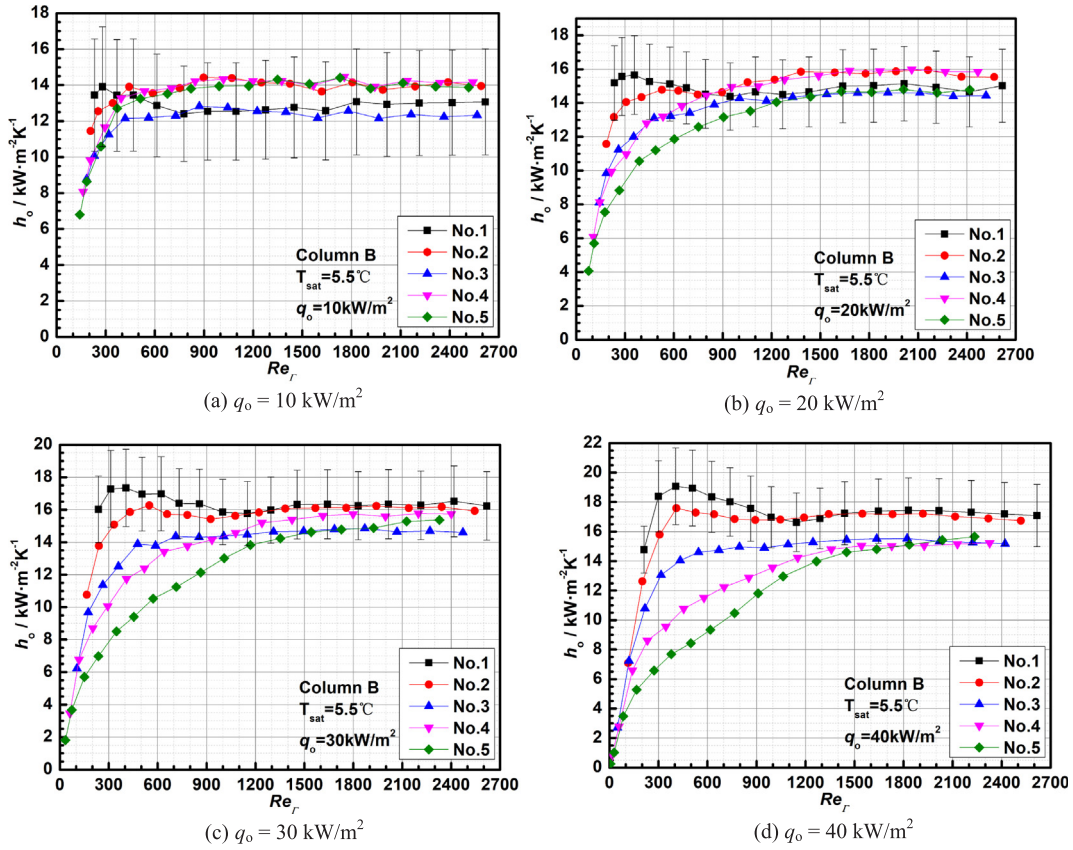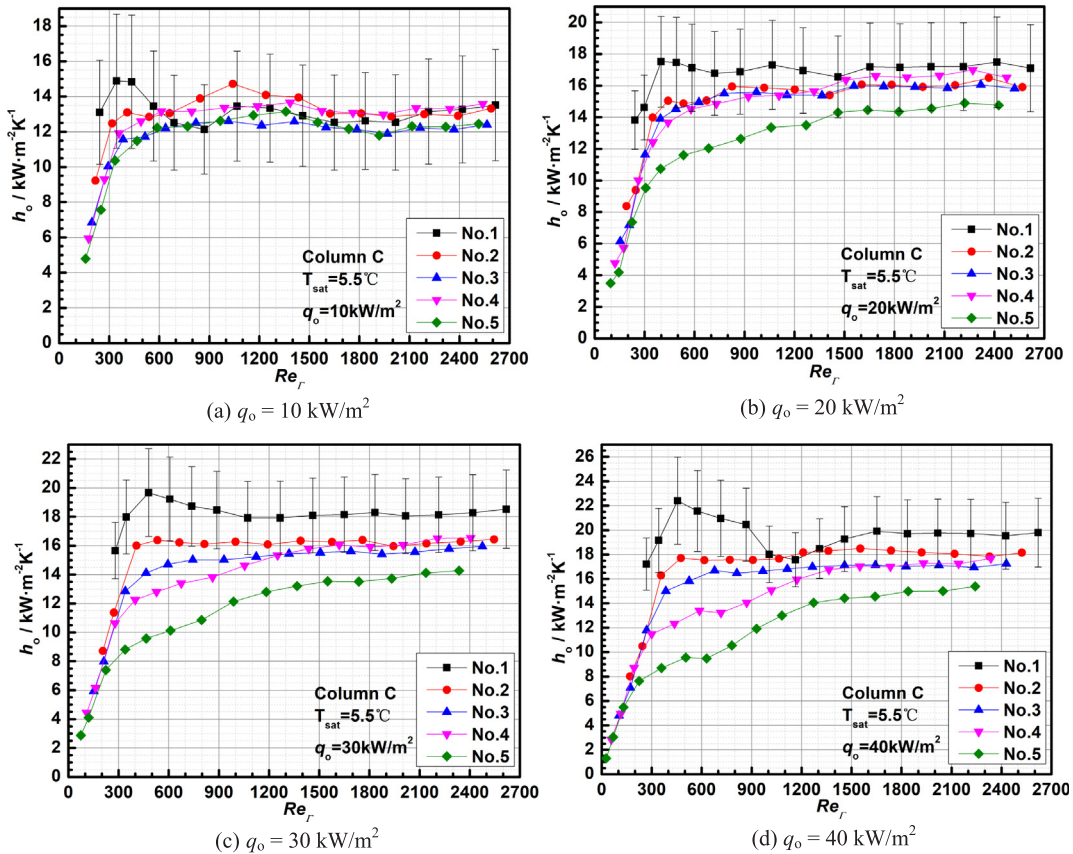
Fig. 10. Variation trend of HTCs with film Reynolds number of column C.
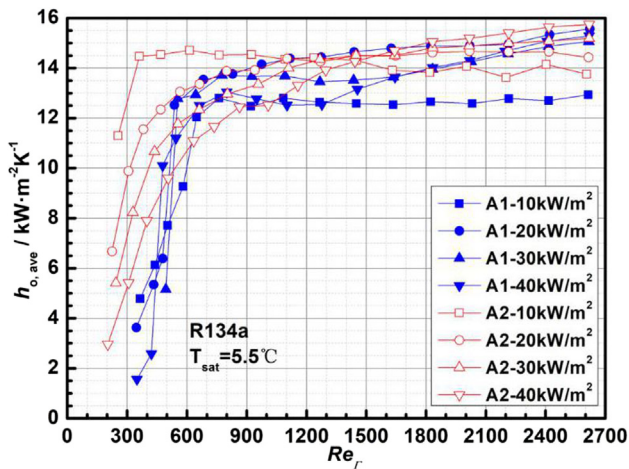
Fig. 11. Comparison of average HTCs between column A1 and A2.
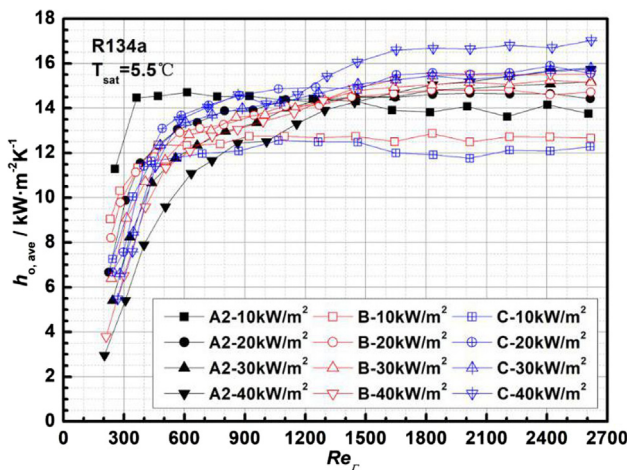
Fig. 12. Comparison of average HTCs among column A2, B and C.

Reynolds numbers are around 600 to 900 except for heat flux of 10 kW/m^2 of column A2.

5) At higher local film Reynolds number range (larger than 1200), the effect of heat flux for tube bundles A2, B and C increases with tube pitch. Tube bundle C owns the largest tube pitch in both vertical and horizontal directions; so that the effect of heat flux on bundle average HTC is also the largest.

5. Conclusions

FFE of R134a on four tube bundles comprised of boiling enhanced tubes was studied experimentally in this paper. Apart from the whole tube bundle test, each tube with different position was also tested. The tube-local film Reynolds number was introduced to show the variation trend of the tube-local HTC with film Reynolds number. Based on the present results and analysis, several conclusions can be drawn as follows:

1. The effect of film Reynolds number on tube HTCs varies with tube position in the same tube bundle. HTC variation curve for the upper tubes of the tube bundle first shows a steady or increasing trend and then a sharp decreasing trend (decreasing film Reynolds number), while HTCs for lower tubes show a constantly diminishing trend.

2. The effect of heat flux on falling film evaporation heat transfer is positive at lower heat flux and negative at larger ones for the single tube tested, indicating the change from convective dominated to boiling dominated evaporation.

3. When the local Re_Γ was used to plot the data, the tubes positioned in lower parts of the tube bundles show similar HTCs and threshold film Reynolds numbers with upper ones at lower heat fluxes (10 kW/m^2 and 20 kW/m^2) while exhibit lower HTCs and larger threshold film Reynolds numbers at larger heat fluxes (30 kW/m^2 and 40 kW/m^2).

4. Among the four tube bundles compared, column A1 owns worst HTCs and largest threshold film Reynolds number, showing that larger counter-current vapor flow can deteriorate the heat transfer of FFE.

5. The effect of heat flux on the bundle averaged HTC increases with tube pitch.

Declaration of Competing Interest

The authors declared that there is no conflict of interest.

Acknowledgement

Appendix A. Supplementary material

Supplementary data to this article can be found online at https://doi.org/10.1016/j.applthermaleng.2020.115006.

References

[1] G. Ribatski, A.M. Jacobi, Falling film evaporation on horizontal tube–a critical review, Int. J. Refrig. 28 (2005) 635–653.

[2] C.Y. Zhao, P.H. Jin, W.T. Ji, et al., Experimental investigations of R134a and R123 falling film evaporation on enhanced horizontal tube, Int. J. Refrig. 75 (2017) 190–203.

[3] P.H. Jin, C.Y. Zhao, W.T. Ji, et al., Experimental investigation of R410A and R32 falling film evaporation on horizontal enhanced tubes, Appl. Therm. Eng. 137 (2018) 739–748.

[4] Pu-Hang Jin, Zhuo Zhang, Ibrahim Mostafa, et al., Heat transfer correlations of refrigerant falling film evaporation on a single horizontal smooth tube, Int. J. Heat Mass Transf. 133 (2019) 96–106.

[5] Daisuke Jige, Hiromasa Miyata, Norihiro Inoue, Falling film evaporation of R1234ze(E) and R245fa on a horizontal smooth tube, Exp. Therm. Fluid Sci. 105 (2019) 58–66.

[6] Wen-Tao Ji, Er-Tao Zhao, Chuang-Yao Zhao, et al., Falling film evaporation and nucleate pool boiling heat transfer of R134a on the same enhanced tube, Appl. Therm. Eng. 147 (2019) 113–121.

[7] Bradley D. Bock, Josua P. Meyer, John R. Thome, Falling film boiling and pool boiling on plain circular tubes: Influence of surface roughness, surface material and saturation temperature on heat transfer and dryout, Exp. Therm Fluid Sci. 109 (2019) 109870.

[8] Liang-Han Chien, Yue-Lin Tsai, Ching-Hung Chang, A study of pool boiling and falling-film vaporization with R-245fa/oil mixtures on horizontal tubes, Int. J. Heat Mass Transf. 133 (2019) 940–950.

[9] J. Fernández-Seara, Á.Á. Pardiñas, Refrigerant falling film evaporation review: description, fluid dynamics and heat transfer, Appl. Therm. Eng. 64 (2014) 155–171.

[10] J.F. Roques, J.R. Thome, Falling films on arrays of horizontal tubes with R-134a, Part I: boiling heat transfer results for four types of tubes, Heat Transfer Eng. 28 (5) (2007) 398–414.

[11] M. Habert, J.R. Thome, Falling-film evaporation on tube bundle with plain and enhanced tubes—part I: experimental results, Exp. Heat Transfer 23 (4) (2010) 259–280.

[12] M. Christians, J.R. Thome, Falling film evaporation on enhanced tubes, part 1: experimental results for pool boiling, onset-of-dryout and falling film evaporation, Int. J. Refrig. 35 (2012) 300–312.

[13] L.H. Chien, Y.L. Tsai, An experimental study of pool boiling and falling film vaporization on horizontal tubes in R-245fa, Appl. Therm. Eng. 31 (2011) 4044–4054.

[14] L.H. Chien, R.H. Chen, An experimental study of falling film evaporation on horizontal tubes using R-134a, J. Mech. 28 (2) (2012) 319–327.

[15] Wen-Tao Ji, Chuang-Yao Zhao, Ding-Cai Zhang, et al., Effect of vapor flow on the falling film evaporation of R134a outside a horizontal tube bundle, Int. J. Heat Mass Transf. 92 (2016) 1171–1181.

[16] C.Y. Zhao, W.T. Ji, P.H. Jin, et al., Cross vapor stream effect on falling film evaporation in horizontal tube bundle using R134a, Heat Transf. Eng. (2017) 1–14.

[17] C.Y. Zhao, W.T. Ji, P.H. Jin, et al., Experimental study of the local and average falling film evaporation coefficients in a horizontal enhanced tube bundle using R134a, Appl. Therm. Eng. 129 (2018) 502–511.

[18] C.Y. Zhao, W.T. Ji, P.H. Jin, et al., Effect of downward vapor stream on falling film evaporation of R134a in a tube bundle, Int. J. Refrig. 89 (2018) 112–121.

[19] E.W. Lemmon, M.L. Huber, M.O. McLinden, Reference fluid thermodynamic and transport properties (REFPROP), Version 8.0, Nat. Inst. Standards Technol. (NIST) (2008).

[20] V. Gnielinski, New equations for heat and mass transfer in the turbulent flow in pipes and channels, Int. Chem. Eng. 16 (1976) 359–368.

[21] V. Gnielinski, On heat transfer in tubes, Int. J. Heat Mass Transf. 63 (2015) 134–140.

[22] S.J. Kline, F.A. McClintock, Describing uncertainties in single-sample experiments, Mech. Eng. 75 (1953) 3–9.

[23] B. Cheng, W.Q. Tao, Experimental study of R-152a film condensation on single horizontal smooth tube and enhanced tubes, ASME J. Heat Transfer 116 (1994) 266–270.

[24] S.M. Yang, W.Q. Tao, Heat Transfer, 4th ed., Higher Education Press, Beijing, China, 2006.

[25] D.C. Zhang, Experimental and numerical investigation of refrigerant condensation and boiling heat transfer characteristics on doubly-enhanced tubes (Ph.D. thesis), School of Energy and Power engineering, Xi'an Jiaotong University, 2007.

[26] Wen-Tao Ji, Ding-Cai Zhang, Ya-Ling He, et al., Prediction of fully developed turbulent heat transfer of internal helically ribbed tubes - An extension of Gnielinski equation, Int. J. Heat Mass Transf. 55 (2012) 1375–1384.

[27] Y.A. Cengel, A.J. Ghajar, Chapter eight: Internal forced convection, Heat and Mass Transfer Fundamentals and Applications, McGraw-Hill, New York, 2011, p. 489.

[28] C.Y. Zhao, Experimental and numerical investigation on the falling film fluid flow and heat transfer outside horizontal tube (Ph.D. thesis), Xi'an Jiaotong University, Xian, China, 2016.